

CONFERENCE ON ELECTRICAL INSULATION  
AND DIELECTRIC PHENOMENA

THE 1980 J. B. WHITEHEAD MEMORIAL LECTURE

INTERFACE EFFECTS IN THE ELECTRICAL RESPONSE  
OF NON-METALLIC CONDUCTING SOLIDS AND LIQUIDS

J. Ross Macdonald  
William R. Kenan, Jr., Professor of Physics  
Department of Physics and Astronomy  
University of North Carolina  
Chapel Hill, North Carolina

JOHN BOSWELL WHITEHEAD

Two of the recent J. B. Whitehead Memorial Lecturers, J. G. Trump and Bernhard Gross, have discussed Whitehead the man, and Gross has touched on Whitehead's work on the anomalous properties of dielectrics, emphasizing and reiterating Whitehead's feeling about the great divergence between the points of view of experimentalists and theorists in the field.

In the National Academy of Sciences Biographical Sketch of Professor Whitehead [1], it tells of his habit of never throwing anything away. He justified this position with the statement, "Keep a thing nine years, and you will find a use for it." As a one-time experimenter in the field of dielectrics and a long-time theorist, I plan today to tell you something about part of the theoretical work of myself and my associates, J. A. Garber, D. R. Franceschetti, and A. P. Lehnen, over the last nine years, without I hope thereby widening the gap between theory and experiment! The principal subject, ac and dc response of solids and liquids, was one close to the heart of John Whitehead, and three of the nine chapters of his 1927 book [2], Lectures on Dielectric Theory and Insulation, deal with dielectric behavior under alternating stress. In fact, his next to last paper [3], was entitled, "The Measurement of Dielectric Loss at High Frequencies and under Changing Temperatures." We are still working today in areas pioneered by Whitehead, and much of his work still repays study for background results and concepts.

## GENERAL BACKGROUND

Starting near the beginning, I remind you that Robert Symmer invented the two-fluid theory of electricity in 1759 by reasoning about the sparks thrown off by his socks! Since then, the field has grown quite a bit, and I must therefore restrict consideration to only a small part of it, the part I know most about. First, let me mention those areas I won't discuss any further.

There is a whole area of great interest encompassing single or double injection of charge at electrodes into an originally nearly insulating material. It is well summarized in the book by Lampert and Mark [4]. Another important area, which is to be the main topic of Session IV later on in this 1980 CEIDP meeting, which was discussed at the 1978 conference by Dr. Gross [5], and which has been reviewed in detail elsewhere by him [6], is that of charge storage and polarization effects in condensed matter induced by penetrating radiation.

The general area which I will discuss is that of the electrical response of a solid or liquid which contains positive and negative charge, with mobile charges of at least one sign. In the solid, immobile charge may be present in addition to mobile charge of one or both signs. In all cases, it is assumed that the material is electrically neutral in the bulk, far away from any electrodes, when the system is in thermal equilibrium with no potential difference  $V_a$  applied across the electrodes.

One interesting approach to the steady-state ac and transient response of materials is that developed in recent years by Jonscher [7] and termed by him, "The Universal Dielectric Response." Such response, frequently found experimentally, is that where the real and imaginary components of the complex dielectric permittivity are proportional to  $\omega^{n-1}$ , where  $0 < n < 1$ . Associated with this frequency response for a linear system is a current transient response, on application of a constant p.d., of the form  $t^{-n}$ . Response of this character was discussed by the author and Brachman [8] in 1956, and it was pointed out there that it was formally physically unrealizable (see also Ref. 9). Nevertheless, this type of response may hold quite well over limited frequency and time ranges, and it was suggested [8] that it might also be related to the  $1/f$  noise found in many electrical devices. One way to cure the defect inherent in the  $t^{-n}$  form is to start instead with the Voglis [10] expression  $[1 + (t/\tau_0)]^{-n}$  and derive the associated frequency response of the system. This approach was followed [11] in 1961, was applied to internal friction and creep rather than electrical response, and led to interesting agreement with a substantial body of data, a considerable part of the agreement being in the region where  $l$  could not be neglected compared to  $(t/\tau_0)$ .

The Jonscher universal dielectric response (UDR) has been proposed to apply to systems with permanent dipoles, and to hopping charge carriers of electronic, polaronic, and ionic nature. It is said to be valid in single crystals, in polycrystalline, and in amorphous structures, universal indeed! It is believed to arise from a variety of ubiquitous correlated states [12]. If this response were indeed as universal and ubiquitous as claimed, this should properly

be my stopping point. At most, universal response theory is probably an alternative, holistic description of the response of some materials which contain free charge to the approach I will discuss, that where the detailed transport, continuity, and Poisson equations are solved with appropriate boundary conditions.

First, I shall discuss fitting and analysis of frequency-response data, including relatively simple electrical equivalent circuits and their possible elements. Next, I shall present a few examples of theoretical small-signal response curve shapes plotted in the complex plane. More shapes, plotted in two and three dimensions and derived from complex least squares fits of various kinds of data, will follow in order to show the utility of this method. Then some results will be presented for transient and frequency response for applied potentials sufficiently large to make the system behave nonlinearly. Finally, nonlinear response will be discussed when the finite size of ions is explicitly taken into account using a lattice gas model for the charged species present in both the bulk and the interphase region.

## FITTING AND ANALYSIS OF DATA

Here I shall discuss small-signal frequency response measurements, leading to impedance  $Z$  or admittance  $Y$  vs frequency, taken at constant temperature. There are two other complex quantities also worth considering: the Modulus function [13]  $M = i\omega Z$  and the complex capacitance function [14,15]  $K = (Y/i\omega)$ . The latter function, when properly normalized, also yields the conventional complex dielectric permittivity function. It is frequently useful to plot some or all of these quantities, or their complex conjugates, in the complex (argand) plane, as parametric functions of frequency. In my opinion, one can usually conclude more from such plots about the physical processes leading to the response and/or the most appropriate equivalent circuit with which to fit the response than from just plotting such quantities as loss tangent or parallel or series capacitance vs frequency. Many examples of complex plane plots will be given later. Another possibility, which I am currently developing, and whose use I most strongly urge, is three-dimensional perspective plotting with axes such as  $\log(f)$ ,  $\text{Re}(Z)$ , and  $-\text{Im}(Z)$ . Results for this new kind of plotting, which can show a great deal of information at a glance, will also be presented later.

Consider the two-dimensional complex plane plot. One would like it to show as much structure as possible, and some of the four functions above show more than others for the same data. For example, if the data involve two time constants whose difference arises primarily from differences in resistances rather than capacitances, a plot of  $M$  shows structure emphasizing the separation of the time constants. On the other hand, if the difference arises primarily from a difference in capacitances, the complex plane plot of  $Z^*$  is most appropriate. Here the star indicates complex conjugation.

Although many authors use complex dielectric permittivity plots (Cole-Cole plots [16]), they are only most appropriate, in my opinion, for true dielectric response, such as that of polar materials without mobile charge. The dielectric permittivity is properly an intensive material parameter, whereas an effective complex dielectric permittivity derived from  $K$  will not be intensive over the entire frequency range if some of the response involves truly mobile charge with or without diffusion effects. In such cases, which are the only ones considered here, it seems much more preferable to deal only with some or all of the four complex quantities mentioned above and investigate the intensive-extensive character of complex plane plots by repeating measurements with different electrode separations  $\ell$ . It seems somewhat inappropriate, for example, for the Jonscher UDR approach to be applied to materials with mobile charges under a name which involves "dielectric."

later, even when the originally unknown values of numerous parameters are to be estimated. Further, it is a completely objective method and yields estimates of both the overall goodness of fit and, quite important, estimates of the uncertainties of the estimated parameters as well.

When equivalent circuits can be employed, a minimum necessary total number of elements should be used and the maximum number of these should be frequency independent (lumped ideal resistances, capacitances, inductances). But different equivalent circuits are not always mathematically unique. Fig. 2 shows three three-time-constant ( $N=3$ ) circuits, all of which can have exactly the same impedance at all frequencies if the values of the elements are selected properly. Such equality can hold for any value of  $N$ . In the third circuit,  $R_\infty$  is the bulk resistance and  $C_g$  the geometrical capacitance, and the "R" and "A" subscripts stand for the interface processes of electrode reaction and adsorption.

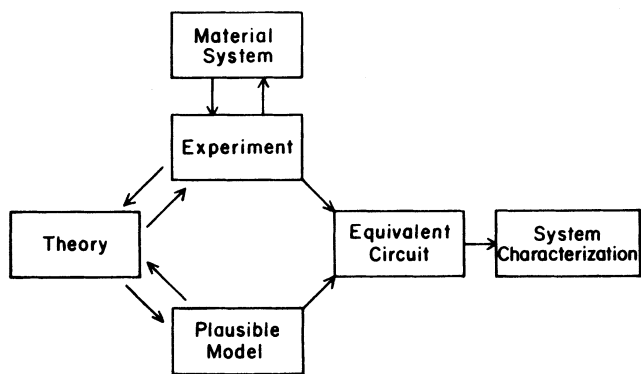


Fig. 1: Block diagram for characterization of a material system

Data and plotting are usually not enough when the object is characterization [17], see Fig. 1. One is then interested in estimates of the parameters which define both the bulk and interface properties of the material. When the theoretical idealized model is sufficiently simple that it can be represented by an equivalent circuit, one will usually want to estimate the parameters which appear in the equivalent circuit first, then use combinations of the results to estimate basic property parameters such as diffusion coefficients, electrode reaction rates, etc. Alternately, some models, including the full small-signal response one [17-19], lead to such complicated complex functions that only in special cases can they be represented by relatively simple equivalent circuits or by useful equivalent circuits at all. In either case, however, parameter estimates may be found by fitting the data to the impedance predicted by the model or the equivalent circuit. I believe by far the best way to do this in both the present mobile charge situation and also in pure dielectric response situations, is to use nonlinear complex least squares fitting [20]. The very high resolution of this method will be demonstrated

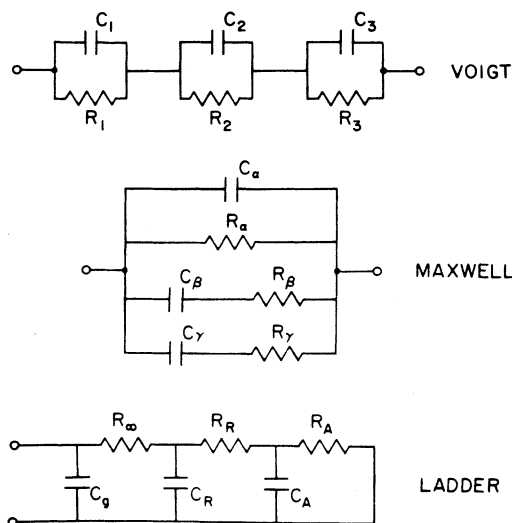


Fig. 2: Three  $N = 3$  circuits which can have the same impedance-frequency relation

How can one choose which circuit ( $N$  to be determined) to use under such conditions? First, the Voigt circuit is probably most appropriate for polycrystalline materials. The Maxwell circuit has been widely used for multiple-time-constant dielectric situations. Finally, the ladder, or continued fraction, circuit is found as a limiting case of the full small-signal model, applicable to liquids or single crystals. It is likely that in any given physical situation the actual connectivity of the system is best represented by a unique circuit. One way to discover which circuit is, in fact, most appropriate is to repeat measurements for different  $\ell$ 's and/or at different temperatures. For a less appropriate circuit, most if

not all of the parameter values will then vary appreciably, while for the most appropriate one some of the parameters may not vary at all, and most if not all of the variation will occur in a minimum set of remaining parameters. Thus, a single fitting of a set of data to a given equivalent circuit will not generally yield estimates of the most appropriate parameters unless the equivalent circuit has already been proven to be the best of those with the same impedance-frequency relation for the situation under study.

Let us now recall that a distributed transmission line of length  $l_e$  has an input impedance of

$$Z(l_e) = Z_0 \frac{Z_o \sinh(X) + Z_{TER} \cosh(X)}{Z_o \cosh(X) + Z_{TER} \sinh(X)}, \quad (1)$$

where  $Z_o \equiv (Z_{ser}/Y_{sh})^{0.5}$ ,  $X \equiv \gamma l_e$ ,  $\gamma \equiv (Z_{ser} Y_{sh})^{0.5}$ , and  $Z_{TER}$  is a terminating impedance. Here  $Z_{ser}$  is the distributed series impedance of the line per unit length,  $Y_{sh}$  is the distributed shunt admittance per unit length, and  $Z_o$  is the characteristic impedance of the line.

A recent treatment [21] of diffusion in electrochemical systems leads to an expression of the form of Eq. (1) with  $Z_{ser} = R_R k_{3b}/D$ ,  $Y_{sh} \equiv i\omega C_{sh} = i\omega/k_{3b} R_R$ , and  $Z_{TER} \equiv R_{TER} = R_R k_{3b}/k_{1ef}$ . Here  $R_R$  is a reaction resistance,  $D$  the diffusion coefficient of the diffusing entity, and the  $k$ 's are rate constants. The total diffusion impedance is found to be  $Z_D = (k_{1b}/k_{3f}) Z(l_e)$ , involving further rate constants. Thus, diffusion can lead to the complex frequency dependence described by Eq. (1) with  $Z_o = R_R k_{3b}/\sqrt{i\omega D}$  and  $\gamma = \sqrt{i\omega/D}$ . Here we are primarily interested in two limiting cases. First is that where  $k_{1ef} = \infty$  and thus the exchange rate of the diffusing entity at the end of the finite transmission line is essentially infinite (since  $R_{TER}$  then equals 0, this is a shorted line). One readily finds that

$$Z_D = Z_{D(SC)} \equiv Z_{D0} \tanh(X)/X, \quad (2)$$

finite Warburg response [17,22]. Here  $Z_{D0} = R_R k_{1b} k_{3b} l_e / D k_{3f}$ . When  $l_e \rightarrow \infty$ ,

$$Z_D = Z_{D\infty} \equiv (R_R k_{1b} k_{3b} / k_{3f}) / \sqrt{i\omega D}, \quad (3)$$

which is the ordinary infinite-length Warburg response [23]. Note that such response is also equivalent to constant phase response with  $n = 0.5$ . Such response, a straight line in the complex  $Z^*$  plane at a  $45^\circ$  angle, is frequently found. If it is, in fact, associated with diffusion, one would expect Eq. (2) to apply at sufficiently low frequencies since no materials are of infinite length. Often frequency response is not extended to low enough frequencies, however, to show the distinction between (2) and (3). At sufficiently low frequencies, (2) shows that the complex  $Z^*$  plane line must curve over to the real axis, yielding a  $\omega \rightarrow 0$  resistance of  $Z_{D0}$ .

The second limiting case, an open-circuited transmission line, is found when  $k_{1ef} = 0$  and the diffusing species is blocked at the end of the line. Then (1) reduces to

$$Z_D = Z_{D(OC)} \equiv (R_R k_{1b} k_{3b} / k_{3f}) \coth(X) / \sqrt{i\omega D}, \quad (4)$$

leading to

$$K_D \equiv (i\omega Z_D)^{-1} = (k_{3f} l_e / R_R k_{1b} k_{3b}) (\tanh(X)/X), \quad (5)$$

similar in form to Eq. (2). But here we are dealing with a completely blocked situation and  $Z_D$  reduces to simple capacitive behavior as  $\omega \rightarrow 0$ .

The finite Warburg appears in diffusion situations where the diffusing species is either neutral (diffusion of a reaction product in an electrode of effective length  $l_e$ ) or is charged in a supporting electrolyte situation ( $l_e = l$ ). For unsupported cases, the full linear model can still yield finite Warburg response under limiting conditions [17]. A complex capacitance of the form of (5) has been derived recently by Glarum and Marshall [24] for a linear model in which mobile charges of one sign are blocked at one electrode but not blocked at the other and charges of opposite sign exhibit opposite blocking/unblocked behavior.

The foregoing results show a few of the possible frequency-dependent elements and responses which may occur and may need to be included in an equivalent circuit. One fairly general one is shown in Fig. 3, where the  $Z_D$ 's are general frequency-dependent elements, such as that involving Eq. (1). Usually only one of the  $Z_D$ 's would appear in a given situation, and that with  $Z_{D1}$  and  $Z_{D2} = 0$  is probably most likely.

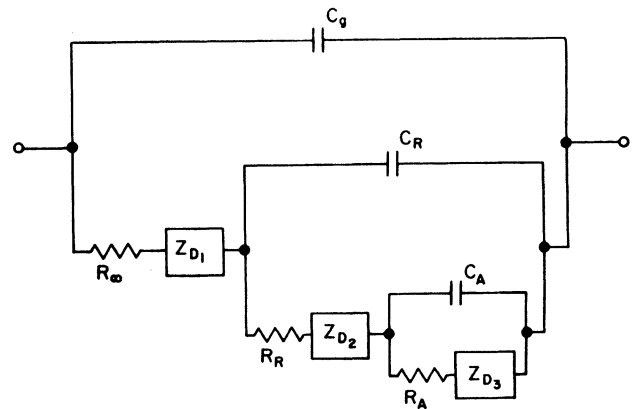


Fig. 3: A general ladder network with three distributed elements,  $Z_{Di}$

LINEARIZED THEORY RESULTS

The solution of the usual continuity, current transport, and Poisson equations with appropriate boundary conditions can be carried out exactly in the flat-band limit when only a vanishingly small ac signal is applied [17,25]. Solutions may be applied to semi-conductors, ionic crystals, and solid and liquid electrolytes. Here I shall concentrate primarily on materials with mobile ions and/or charged imperfections. Although the theory includes arbitrary charge valences, only the usual univalent situation will be discussed here. The following physical processes are usually included in the theory, and some or all of them may be important in specific cases:

- Charge transport: conduction and diffusion
- Generation/Recombination: of charged species
- Neutral species transport: diffusion in material and/or electrodes
- Adsorption/Desorption: at electrodes
- Charge transfer (redox reactions): at electrodes.

The first two of these processes are homogeneous and occur in the bulk (but diffusion is intensive at high frequencies and extensive at low); the last two are heterogeneous (intensive) interface processes, and the middle one is a homogeneous process occurring in either the bulk or in the electrode (or possibly both). A diagram showing the interaction of some of the processes present in an electrode/material situation is presented in Figure 4. Here the compact or Stern layer is by definition either charge free or contains specifically adsorbed charges only.

The selection of appropriate boundary conditions is usually of critical importance in developing a useful theoretical model to compare with specific experimental results. The Chang-Jaffé conditions [15,17,18, 25] have often been used when electrodes are not completely blocking to charge transfer. These conditions state that at an electrode surface the perpendicular convection current carried by a given charged species is proportional to the difference between the concentration of the species at the boundary and its concentration in the bulk in equilibrium. More realistic conditions for ionic materials are the Butler-Volmer relations [18,26] which take some account of the effect of the finite size of ions at the boundary.

Many and varied are the forms of small-signal model frequency response results when plotted in the  $Z^*$  or  $Y$  complex planes. When the time constants of the various processes are relatively close together the resulting shapes can be quite complicated. Many shapes are illustrated in Refs. 15, 27, 28, and in the two reviews, Refs. 29 and 30. Here I reproduce in Figs. 5-7 some  $Z^*$  and  $Y$  shapes for various conditions, together with their associated equivalent circuits [28]. Arrows show the direction of increasing frequency. The  $Y_W$  of Fig. 6a is the present  $Z_{D(sc)}^{-1}$ . Although the  $N \geq 2$  RC circuits of Figs. 5 and 6 may be replaced by their Maxwell or ladder equivalents, such replacement is generally invalid when a circuit section involves  $Z_D$  rather than a  $R$  and  $C$ . The error of taking as equivalent, different circuits containing  $Z_D$  becomes larger the closer the RC time constant approaches the effective time constant of the  $Z_D$  circuit. In the limit where complex  $Z^*$ -plane-shapes arising from these processes don't overlap, the error approaches zero. As an example of a medium-overlap situation, consider the circuit of Fig. 6a with  $R_\infty = 10^3 \Omega$ ,  $C_g = 6 \times 10^{-8} F$ ,  $Z_{D0} = 4 \times 10^3 \Omega$ , and  $H = 0.06$ . Here I have set the  $v_e^2/D$  which appears in the  $X$  variable of  $Z_{D(sc)}$  equal to  $H^2$ . Synthetic data were generated for this circuit and a complex least squares fit of these data to the Fig. 3 ladder circuit with  $Z_{D1} = Z_{D(sc)}$ ,  $C_R = R_R = Z_{D2} = R_A = C_A = Z_{D3} = 0$  was attempted. No adequate fit could be found with the most appropriate weighting, but unity weighting of the data yielded the estimates  $R_\infty \cong (1229 \pm 17)$ ,  $10^8 C_g \cong (2.645 \pm 0.045)$ ,  $Z_{D0} \cong (3701 \pm 18)$ , and  $H \cong (0.0584 \pm 0.0003)$ . Although most of these estimates are fairly close to the original values, this fit is very poor compared to that obtained with the original circuit, which led to essentially exact estimates of the original parameters. The present fit yields relative deviations between data and circuit predictions that approach 100% for frequencies greater than about  $4 \times 10^3$  Hz.

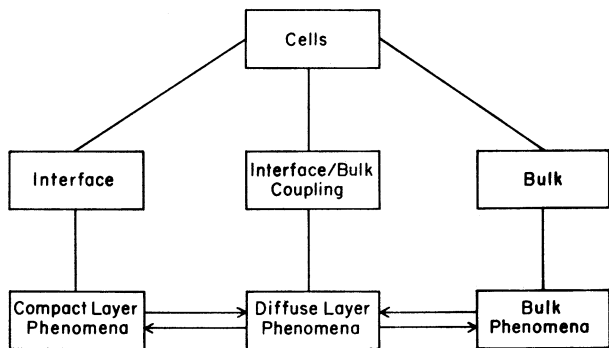


Fig. 4: Block diagram showing some bulk-interphase relations

Fig. 7 shows bulk (B), reaction (R), and adsorption/reaction (A/R) semicircular shapes for different electrode rate constant parameters. In the A/R case, it has proven very useful to employ complex rate constants [18,31]. Note that those curves with arrows pointing to the right in Fig. 7 involve negative A/R differential resistances ( $R_A < 0$ ), and those curves with  $\text{Im}(Z_T^*) < 0$  involve negative differential capacitances ( $C_A < 0$ ) as well.

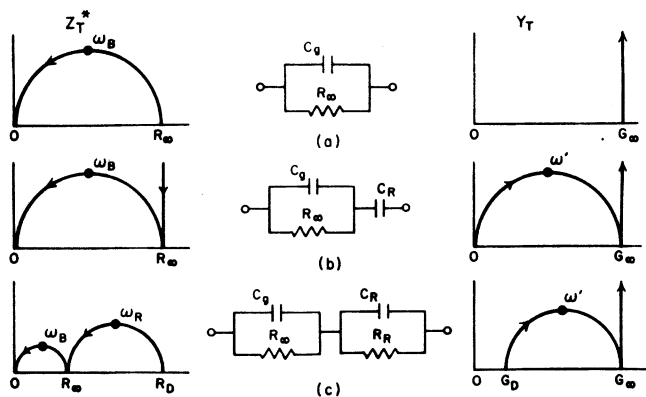


Fig. 5:  $Z^*$  and  $Y$  plane responses for several simple equivalent circuits

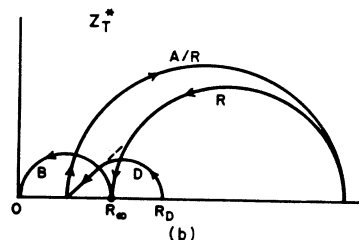
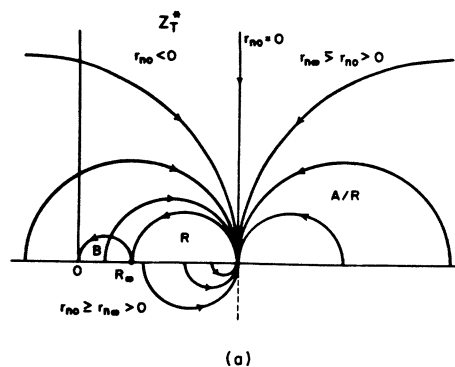


Fig. 7:  $Z^*$  and  $Y$  plane responses for situations involving adsorption/reaction processes. In (a) the  $r_n$ 's are normalized reaction parameters [28]. The curves presented in (b) include finite Warburg response, denoted  $D$  here.

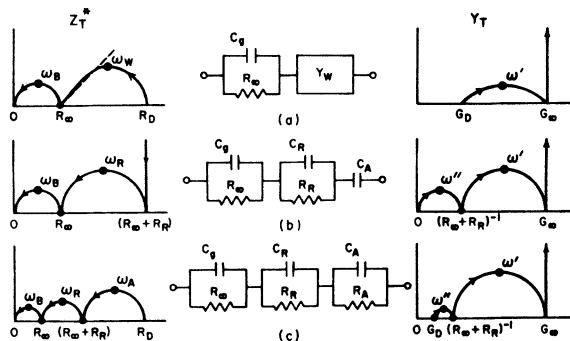


Fig. 6:  $Z^*$  and  $Y$  plane responses for more complex equivalent circuits

Let us denote diffusion response such as that arising from  $Z_D(SC)$  of Eq. (2) by  $D_S$  and the  $Z_D(OC)$  of Eq. (4) by  $D_O$ . When  $l_e \rightarrow \infty$ , they both reduce to the  $Z_{D\infty}$  of Eq. (3), which we will denote by  $D_\infty$ . In addition, denote a capacitive element by  $C$ , and the constant phase element by  $CPE$ . How may these be combined to yield various shapes in the complex plane? Consider the circuit of Fig. 3 with  $Z_{D1} = Z_{D2} = 0$ , for example. It can give the shapes of Fig. 7b if  $R_A$  is negative and  $Z_{D3} = Z_D(SC)$ . Thus this  $Z^*$  plane response may be represented symbolically by  $B-R-A/R-D_S$ , moving from high frequencies to low. The shortest effective time constant sections come first and the longest last, but clumping of time constants can lead to much more complicated results.

We always find that  $B$  comes first in any such sequence. Often measurements are not extended to sufficiently high frequencies to allow its  $C$ , the geometric capacitance  $C_g$ , to be obtained. Then after  $B$  follows the  $R$ ,  $A/R$ , or  $D_S$  which has the smallest effective time constant. If  $R$  and  $A/R$  are both non-zero, they occur in the  $R$ ,  $A/R$  sequence since they involve sequential processes. Thus, such responses as  $B-D_S-A/R$ ,  $B-R-D_S-A/R$ , and  $B-R-A/R-C$  are possible. In Fig. 3, the first of these would require  $Z_{D2} = Z_{D3} = 0$  and  $Z_{D1} = D_S$ , while the second would involve  $Z_{D1} = Z_{D3} = 0$  with  $Z_{D2} = D_S$ . As illustrated above,  $C$  must come last, as in Fig. 5b, when it is the only blocking element. Similarly, since  $D_0$  reduces to simple capacitive behavior as  $\omega \rightarrow 0$ , it must come last if it provides the only blocking. When both  $D_0$  and  $C$  occur, their order is not significant. Note that  $CPE$  or  $D_\infty$  response may be substituted for  $D_S$  in the above, but the overall response will then still exhibit a kind of blocking behavior since  $\text{Re}(Z^*)$  will increase without limit as  $\omega \rightarrow 0$ , eliminating any dc path through the circuit. Incidentally, many of the sequences discussed above have been found experimentally, even that of the rather complex Fig. 7b [32]. Of course such complex shapes are not predicted by the UDR. Some transient and frequency-response results for cases where generation-recombination of extrinsic charge carriers is important have also been presented [33] but the effects of generation/recombination are often subtle compared to those of some of the other processes included in the linearized theory [17].

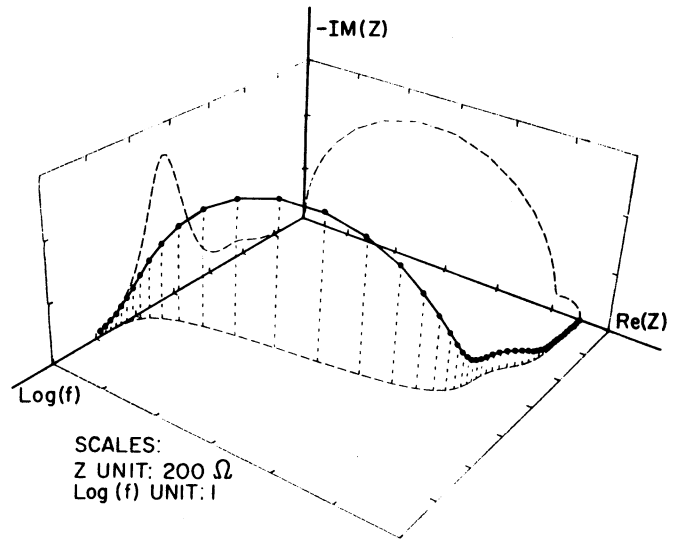


Fig. 8: Perspective 3-D  $Z^*$  response of an  $N = 2$  Voigt circuit. Two-dimensional projections shown dashed.

SOME COMPLEX-LEAST-SQUARES FITTING RESULTS

In this section, results for three different types of situations will be summarized: first, complex least squares fitting with synthetic data generated from a known circuit with known parameters; second, fitting of experimental data obtained from a known circuit of actual  $R$ 's and  $C$ 's only; and third, fitting of experimental data for a single crystal of  $\text{PbF}_2$ .

The three-dimensional impedance-frequency plot with perspective presented in Fig. 8 shows response of a particular realization of the  $N = 2$  circuit of Fig. 5c. The actual "data" points used in the plotting are shown in Fig. 8 connected by straight line segments. The origin of the  $\log(f)$  scale is taken at  $-1$  here and in the succeeding 3-D plots, equivalent to  $f = 0.1$  Hz, and the highest frequency point plotted here is at 75 kHz. The origin values of the  $Z$  axes are zero here. Note how much more clearly the frequency separation between time constants shows up in the 3-D as compared to the ordinary 2-D  $Z^*$  complex plane plot (the back projection here). When color is also available, 3-D plots will be even more useful. The data presented in Fig. 8 were calculated with  $R_\infty = 10^3 \Omega$ ,  $C_g = 0.1 \mu\text{F}$ ,  $R_R = 100 \Omega$ , and  $C_R = 100 \mu\text{F}$ . The points shown are equally spaced in log frequency (frequency ratio  $10^{1/8}$ ) starting at  $f = 0.1$  Hz. These parameter values yield a time constant ratio of 100 and a 10:1 difference in the size of the two arcs. How well can one resolve data like this using nonlinear complex least squares fitting? To approximate experimental results, the exact calculated  $\text{Re}(Z)$  and  $-\text{Im}(Z)$  data values were truncated to lengths of  $n = 4, 3$ , and 2 total digits. The last of these gives modified data results of no better than 10% relative accuracy on the average.

Table I. Complex least squares fitting results for the data depicted in Figure 8

Weighting Type	n	$R_\infty$	$10^7 C_g$	$R_R$	$10^4 C_R$
0	3	1000.04 ± 0.28	1.00015 ± $7 \times 10^{-4}$	100.28 ± 0.34	1.0177 ± 0.0094
P	3	999.78 ± 0.19	1.00011 ± $2 \times 10^{-4}$	100.02 ± 0.06	0.9999 ± 0.0012
P	2	999.28 ± 1.69	1.0028 ± 0.0017	99.83 ± 0.51	0.998 ± 0.010

Complex least squares fitting was carried out both for unweighted (actually unity weighted) data ( $w \equiv 0$ ) and with the assumption that the random errors in the data were proportional to the magnitudes of the data values ( $w \equiv P$ ). As one might expect, the latter generally gave better results. Table 1 shows some of the  $Z$ -fitting parameter estimates and their estimated uncertainties (standard deviations) for several situations. Even with  $n = 2$ , quite good results for all parameter estimates are found for these data.

Table II. Complex least squares fitting results for a different  $N = 2$  situation (see text)

$n$	$R_{\infty}$	$10^5 C_g$	$R_R$	$10^3 C_R$
4	1000.39 $\pm 0.44$	1.9989 $\pm 0.0013$	9.58 $\pm 0.43$	1.031 $\pm 0.034$
3	1005.7 $\pm 1.6$	1.9828 $\pm 0.0050$	4.38 $\pm 1.48$	1.78 $\pm 0.40$
3	1001.8 $\pm 1.7$	1.9959 $\pm 0.0051$	8.35 $\pm 1.73$	1.13 $\pm 0.17$
2	1007.2 $\pm 3.3$	1.975 $\pm 0.013$	1.22 $\pm 1.91$	3.12 $\pm 2.79$

Next, a much more stringent least squares resolution was attempted. Here the values of  $R_{\infty}$ ,  $C_g$ ,  $R_R$ , and  $C_R$  used to calculate exact "data" were  $10^3 \Omega$ ,  $20 \mu\text{F}$ ,  $10 \Omega$ , and  $10^3 \mu\text{F}$ . These values yield a time-constant ratio of only 2 and a size ratio of 100:1. Table 2 shows a few fitting results for this situation, all with  $W=P$  weighting. The 32 data points used here began at  $f = 0.1$  Hz and extended to about 750 Hz with uniform spacing in log frequency, frequency ratio  $10^{1/8}$ . We see that reasonable results are obtained, even for  $R_R$  and  $C_R$  with  $n = 4$ . In Table 2 all results are again for fitting of  $Z$  data except the second  $n = 3$  row, a  $Y$  fit. These  $Y$  fitting results were obtained by fitting of  $Y$  data generated by inverting the exact  $Z$  data and then truncating to  $n = 3$ . They happen to yield somewhat better estimates here, though this is not by any means always found to be the case. For  $n = 3$ , the truncated "data" are not really quite accurate enough to yield a good estimate of  $R_R$  although the actual  $Y$ -fit estimate of  $R_R$  is within less than two of its standard deviations of the correct value. Here when  $n = 2$ , the values of  $R_R$  and  $C_R$  obtained from  $Z$  or  $Y$  fits are wholly uncertain. I believe that these and similar results show that the resolution of complex least squares fitting can be very high even for typical 1% data, provided that a sufficient frequency region is covered. Note that the method may also be used to resolve nearly overlapping Debye curves for complex dielectric permittivity or  $K$  data.

The frequency response of the actual  $N = 3$  ladder network of Fig. 9 was measured by Dr. J. Schoonman of the University of Utrecht using a Solartron type 1172 response analyzer (private communication). Here the real values of  $Y$  had four decimal digits and the imaginary parts had either three or four. Frequencies were equally spaced in  $\log(f)$  with a ratio of about 1.58 and extended from 0.4 Hz to  $10^4$  Hz. Nominal values of the lumped circuit elements used are shown on the figure (top values), with resistances in  $\Omega$  and capacitances in nF. Measured  $Z^*$  vs  $f$  points are plotted in 3-D for both  $Z$  and  $Y$  in Figs. 10 and 11 using different viewing directions for maximum clarity.

Here the origin of the  $\text{Re}(Z)$  axis is at  $2.5 \text{ k}\Omega$ , and in Fig. 11 the origin of the  $\text{Re}(Y)$  axis is at  $120 \mu\text{S}$ . As usual, the origins of the imaginary axes are at zero. We see very little separation in Figs. 10 and 11 between the sections of  $2.75 \times 10^{-5}$  and  $2.11 \times 10^{-4}$  sec. time constants even though their ratio is about 7.7. Unity weighting proved to yield results with smaller parameter standard deviations for these data than did proportional weighting. Parameter estimates found from  $Y$  fitting are those shown in parentheses in Fig. 9.

These results show good agreement with the nominal values. It is likely that the least squares estimates are, in fact, appreciably more accurate than the nominal values since the former represent the result of many individual measurements. As a check, the capacitor  $C_R$  was measured at  $f = 120$  to  $10^3$  Hz by Schoonman (private communication) using a General Radio type 1680 bridge, yielding values which ranged from about 11.9 to 12.25 nF with some slight tendency toward increasing values with increasing frequency. The mean and standard deviation of nine measurements was  $12.09 \pm 0.15$  nF, in close agreement with the fitting result. Fitting to data in impedance rather than admittance form gave parameter estimates very close to the above values but with appreciably larger parameter standard deviations. There is no point in showing a comparison between the original data and values predicted from the fit since relative errors were generally in the range of  $10^{-3}$  to  $10^{-4}$ .

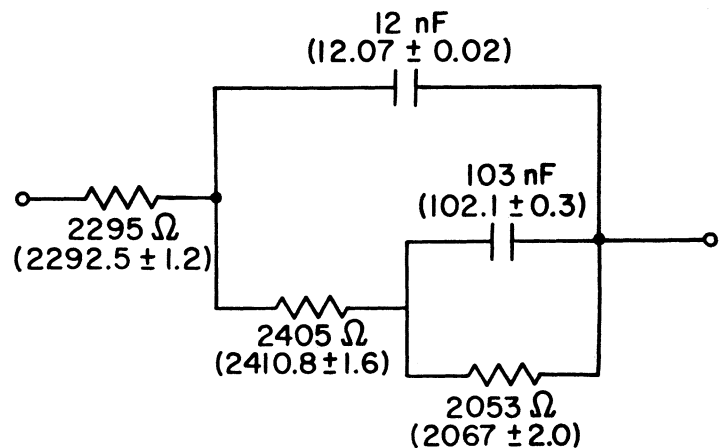


Fig. 9: Test circuit involving lumped elements. Nominal values above, complex least squares estimates and standard deviations in parentheses.

Let us now consider some response data obtained by Schoonman (private communication) on  $\beta$ -PbF<sub>2</sub> with platinum paint electrodes at 474 K. Both  $\text{Re}(Y)$  and  $\text{Im}(Y)$  were given to four decimal places and 27 points spanned the range from 0.2 Hz to 20 kHz. As usual, frequency values were taken to be exact. The circuit employed for fitting was that of Fig. 3 with  $C_g$ ,  $Z_{D1}$ , and  $Z_{D2}$  zero and  $Z_{D3}$  given by a CPE. Weighting of P-type was used and a Z fit gave excellent results. Parameter estimates found were  $R = (2280 \pm 16)$ ,  $R_R = (1931 \pm 55)$ ,  $C_R = (13.29 \pm 0.24)$ ,  $R_A = (890 \pm 40)$ ,  $C_A = (41.6 \pm 3.3)$ ,  $A = (2.196 \pm 0.008) \times 10^{-5}$ , and  $n = (0.4025 \pm 0.0018)$ . The last two estimates refer to CPE parameters. The capacitance  $C_g$  was undeterminable from the data. Here resistances are again in  $\Omega$  and capacitances in nF. Note the desirably small values of parameter uncertainty estimates even when seven parameters whose values were initially unknown are estimated here. The data were also fitted with the same circuit except with  $Z_{D3} = Z_{D(SC)}$ , and the overall standard deviation of fit was found to be nearly eight times larger than that obtained using the CPE.

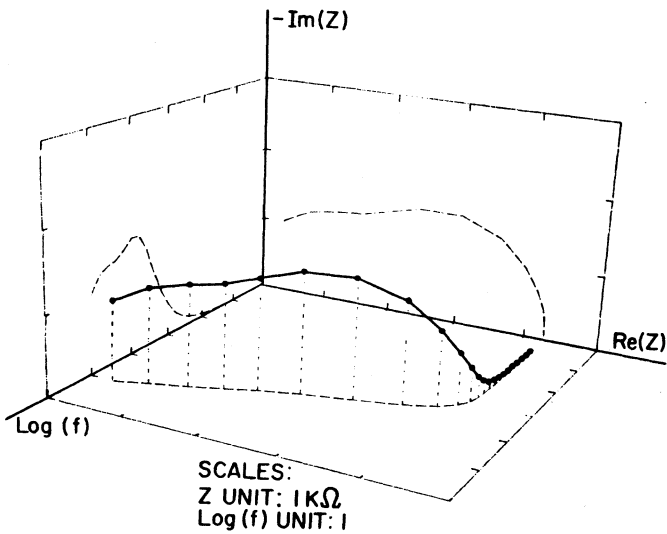


Fig. 10: Perspective 3-D  $Z^*$  response of the circuit of Fig. 9.

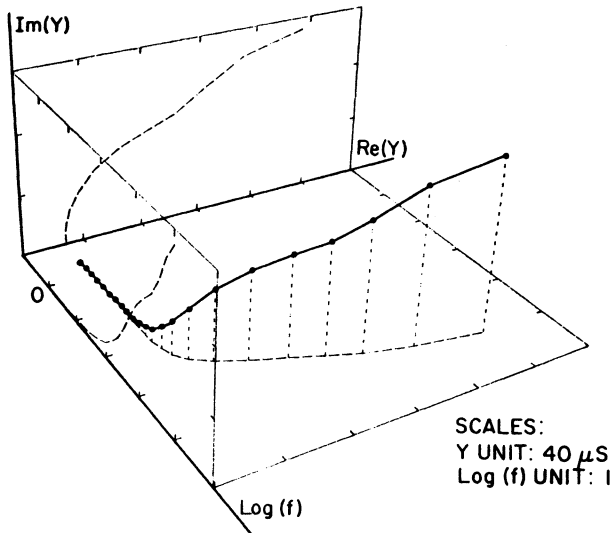


Fig. 11: Perspective 3-D  $Y$  response of the circuit of Fig. 9.

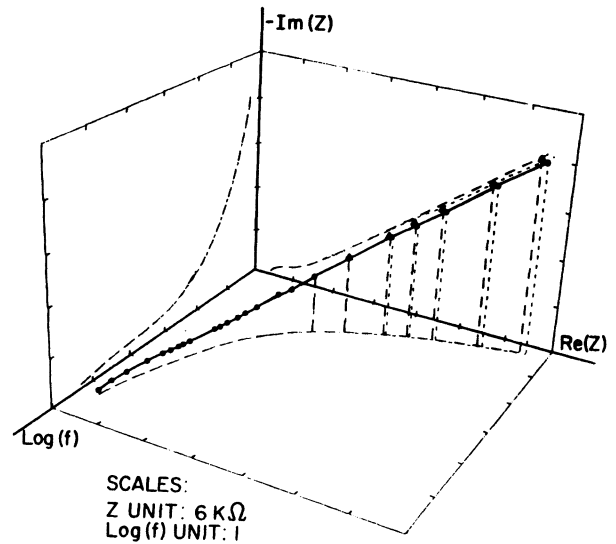


Fig. 12: Perspective 3-D  $Z^*$  response of equivalent circuit data of J. Schoonman on  $\beta$ -PbF<sub>2</sub> at 474 K. Data points are indicated by solid circles and complex least squares fitting results by solid triangles.

Actual complex least squares fitting results are shown in the 3-D  $Z^*$  plot of Fig. 12. Here the original data points are indicated by small solid circles (solid 3-D line) while points at the same frequencies calculated using the CPE-fit parameter estimates are designated by small solid triangles. Most of the original and calculated points fall so close together that they cannot be distinguished. Only at the lowest frequencies do some differences, whose relative sizes are two percent or less, appear. The lines with short dashes are associated with the original data and those with longer dashes with the calculated points.

one sign is mobile. For equal mobilities instead, the relative p.d. dependence of the  $M=10$  curve is reversed over that shown here [34]; that is, slower decay is found with higher  $V_a$  magnitudes. These decay curves are only exponential in the long-time region. None of them is of the  $t^{-n}$  or Voglis response forms. Fig. 14 shows a comparison of charging and discharging curves for the same situation and  $V_a^* = 5$ . Nonlinearity is indicated here by the difference between charging and discharging curves.

Fig. 15 shows normalized small-signal ac frequency response [35], plotted in the complex  $Z^*$  and  $Y$  planes, for the same situation considered above with  $M=10$ . Here the system is biased by the static potential  $V_a$  which determines the space charge distribution in the interface regions and thus the frequency response. Fig. 16 is similar except that it was calculated for one blocking and one ohmic electrode and positive and negative charges are taken to have the same mobility. One sees quite different p.d.-shape dependence for this situation where only a single interface region is important. Further changes in the ratios of the mobilities of the positive and negative charged species lead to large changes in the curve shapes as well [35].

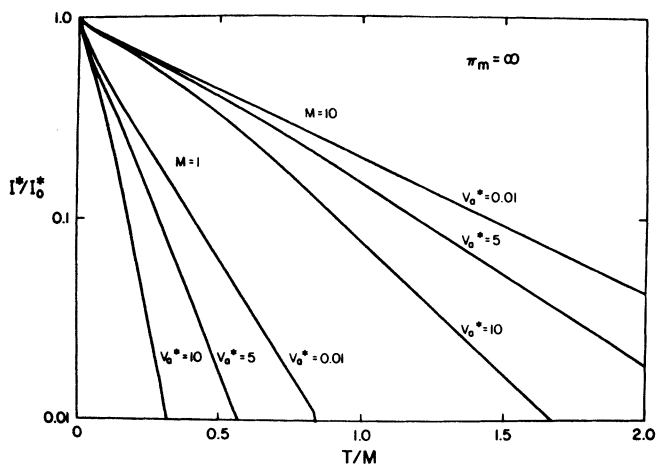


Fig. 13: Normalized current-time charging curves for two different normalized lengths and several step potentials applied at  $t = 0$ . Blocking electrodes present, charge of only one sign mobile.

### NONLINEAR RESPONSE RESULTS

The electrical response of charge-containing materials generally becomes nonlinear when a potential difference of magnitude  $(kT/e)$  or greater appears across a blocking or partially blocking electrode-interface region. Linearization is then invalid, and the full nonlinear, coupled partial-differential charge transport equations must be solved numerically with appropriate boundary conditions to obtain time or frequency response. An accurate computer simulation technique for the solution of such equations has been developed, and the some nonlinear-situation results have already been presented [26,34,35]. Here a few of these results will be discussed.

Consider first the transient response of a simple system made up of intrinsic material without recombination of free charge, fitted with completely blocking electrodes. Let  $V_a^* \equiv V_a/(kT/e)$ , a normalized applied p.d. Fig. 13 shows the normalized charging current vs normalized time obtained [34] for two different lengths upon application at  $t = 0$  of a step-function p.d. of  $V_a$ . Here  $M \equiv l/2L_D$ , where  $l$  is, as usual, the electrode separation and  $L_D$  is the bulk Debye length. These results are for a situation where charge of only

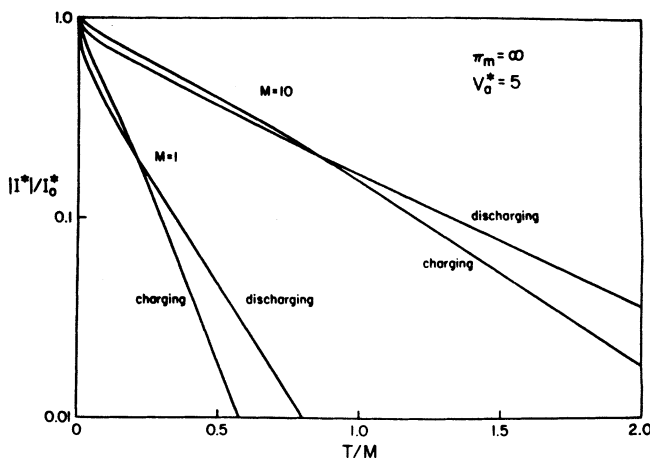


Fig. 14: Normalized current-time charging and discharging curves for two different lengths, demonstrating nonlinear response.

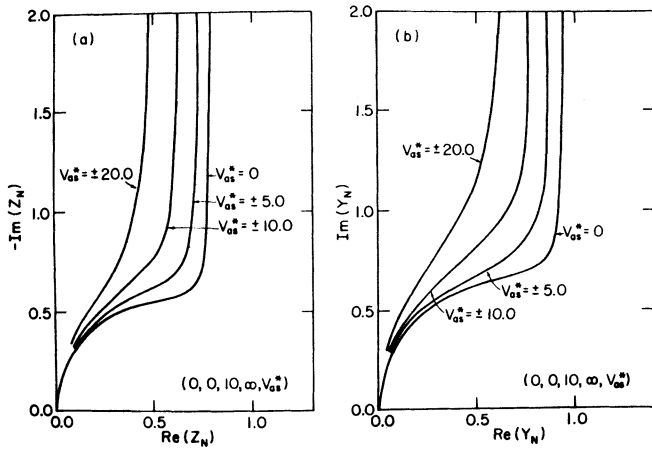


Fig. 15:  $Z^*$  and  $Y$  plane responses for a material with two blocking electrodes as a function of normalized static potential difference across the electrodes,  $V_{0s}^*$ . Charge of only one sign mobile. Normalized impedance  $Z_N \equiv Z/R_\infty$ .

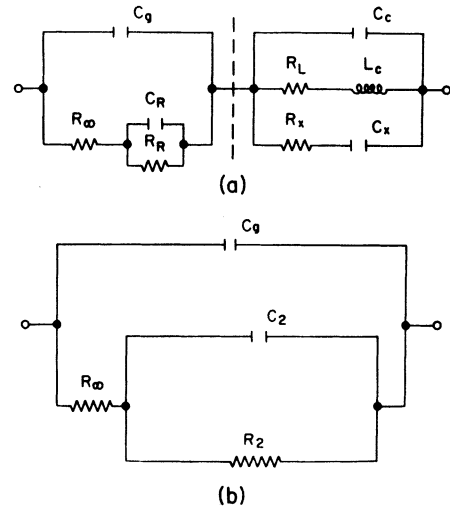


Fig. 17: Unbiased small-signal-response approximate equivalent circuits for material with two partially blocking electrodes; charge of only one sign mobile. Effect of finite ion size in the compact layer shown at right of center in (a).

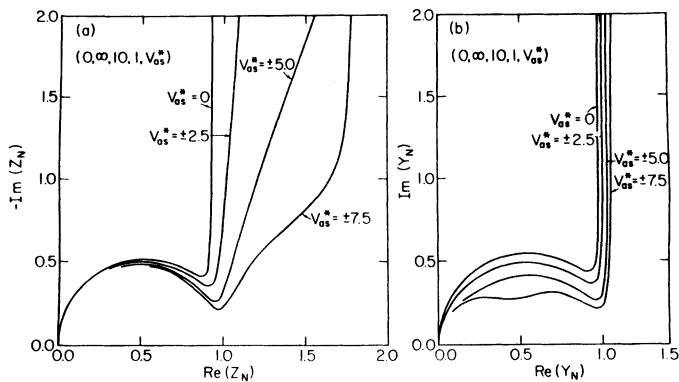


Fig. 16:  $Z^*$  and  $Y$  plane responses for one blocking and one ohmic electrode under static bias; charges of both signs have equal mobilities.

Thus far we have examined the frequency-response complex plane shapes for blocking situations which allow no steady currents. Let us now consider systems with two partially blocking electrodes (A), or with one ohmic and one partially blocking (partially polarizable) electrode (B) with only positive charge mobile. Further, let us take some account of the finite size of positive charges, assumed to be ions, by including a compact or Stern layer next to partially blocking electrodes. No specific adsorption at the electrodes is assumed, but charges must pass through the compact layer in order for an electrode reaction to occur and a steady current to flow. Even the linearized equations lead to a very complicated exact solution for the impedance in the A case [18,19]. An approximate, but still quite accurate, equivalent circuit following from this solution is shown in Fig. 17a. Specific compact layer contributions appear at the right of center. Luckily, it has been found [19] that this circuit reduces with quite high accuracy to the conventional ladder circuit of Fig. 17b. Here  $C_2$  is made up of the diffuse double layer space charge capacitance,  $C_R$ , in series with that of the inner compact layer. See Fig. 5c for the small-signal complex plane shapes to be expected for this circuit.

Now what happens under bias sufficiently large to make the response nonlinear? Fig. 18 shows Case B numerical-solution results for steady-state normalized overpotential-current relations when Butler-Volmer boundary conditions are employed [26]. Here  $K_D$  is a normalized reaction rate constant;  $\alpha$  is the conventional symmetry factor of Butler-Volmer kinetics; and  $\delta$  is the ratio of zero-bias diffuse layer capacitance to compact

layer capacitance. It thus depends on the bulk charge concentration. There is no compact layer present (Chang-Jaffé boundary conditions) when  $\delta = 0$ . The overpotential is defined here as the difference between the total potential and the ohmic potential drop in the material; it is thus the p.d. across the interphase region at the partially blocking electrode. The non-linearity in these current-voltage curves is clear. Notice also how the curves change as  $\delta$  increases and compact-layer effects become more important. The larger the current and overpotential, the more difference there will be between the results of Chang-Jaffé and Butler-Volmer kinetics.

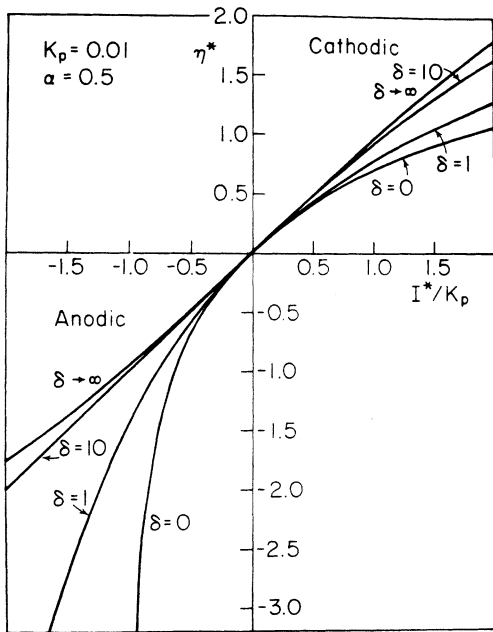


Fig. 18: Steady-state (normalized) overpotential-current relations; one partially blocking electrode with Butler-Volmer kinetics and one ohmic electrode; charge of only one sign mobile. Here  $\delta$  is the ratio of zero-bias diffuse layer capacitance to compact layer capacitance.

Finally, Figs. 19 and 20 present some  $K_p=0.01$  complex  $Z^*$ -plane results for  $M=20$ /Case B and  $M=100$ /Case A situations, respectively. To quite good approximation, these shapes are also well fitted [26] by the circuit of Fig. 17b. Although nonlinearity does not appreciably affect the structure of the circuit here (its connectivity and type of elements), one does find that  $C_2$  and  $R_2$  are current and overpotential-dependent. As Fig. 19 indicates,  $R_2$  increases as the half-cell system goes from having an accumulation region ( $I_s^* > 0$ ) to a depletion region ( $I_s^* < 0$ ). The capacitance  $C_2$  simultaneously decreases as would be expected. The situation is more complex in the Case A situation of Fig. 20 where an accumulation region forms at one

electrode and a depletion region simultaneously appears at the other. The latter dominates the behavior of the overall  $R_2$  of course. Notice that a current of  $I_s^* = 0.02$  is necessary to double  $R_2$  over its unbiased value in the A case while only a change of  $|I_s^*| = 0.01$  is necessary for the case B situation. These results show that when the current is non-zero it would be quite incorrect to derive a reaction rate constant from a value of  $R_2$  using the usual zero-bias relation between the two [18,19], which becomes for case B,  $k_p \equiv K_p D_p / L D = (kT/e) / (e c_0 R_2)$ , where  $k_p$  is not normalized and  $c_0$  is the equilibrium bulk concentration of the positive charge.

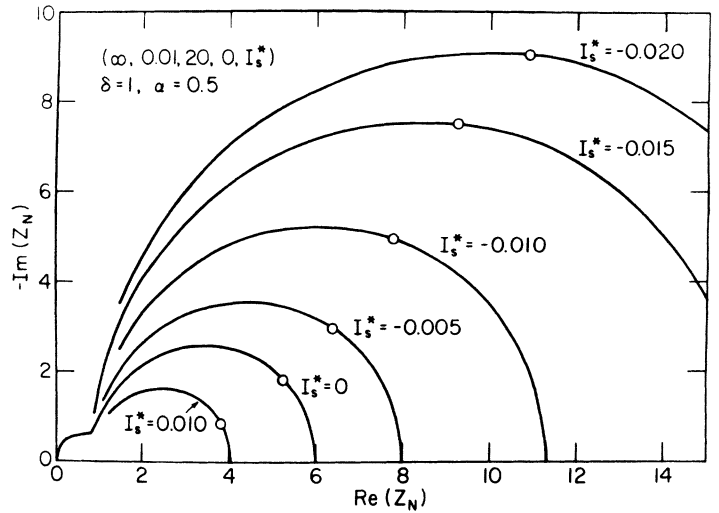


Fig. 19: Small-signal  $Z^*$  plane response under static bias for the situation of Fig. 18 with  $K_p = 0.01$ . The  $I_s^*$  parameter is the normalized steady-state current.

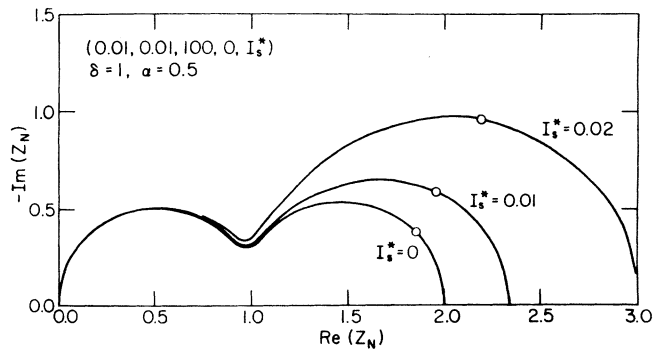


Fig. 20: Small-signal  $Z^*$  plane response under static bias for two partially blocking electrodes with Butler-Volmer kinetics;  $K_p = 0.01$  and charge of only one sign is mobile.

FINITE SIZE EFFECTS

Thus far we have considered one aspect of the finite size of charge carriers in defect or ionically conducting materials, namely the finite thickness of the inner compact layer. But occasions can often arise where finite size enters in another way, leading to a limitation on the maximum two- or three-dimensional concentrations possible in a given region. One expects that such a limitation will be important in systems with very high concentrations or even in those whose equilibrium bulk concentrations are low but where accumulation-type diffuse space charge regions form. In contrast, the conventional Gouy-Chapman theory of the diffuse double layer [36,37] employs an independent-particle ideal gas model (IGM) for the charges, all taken infinitesimally small.

In an effort to overcome some of the limitations of the IGM, which can lead to arbitrarily large charge concentrations, we have begun to explore some of the predictions of various lattice gas models (LGM) [38, 39]. In such models one assumes that the charges must reside on one (liquid model) or two (solid model) lattices of site concentration  $N$ . Then charge concentration of a given sign can never exceed  $N$ , a quantity entirely geometrically determined. Here for simplicity we have considered that the charge carriers of opposite sign are sufficiently close to the same diameter that a site can be occupied by either in the liquid model or that there are  $N$  sites for positive and  $N$  for negative charges in the solid model. The latter is particularly appropriate for single crystals; the version discussed here is applicable for Schottky-defect materials, while somewhat more complexity arises for Frenkel-defect ones [39]. The LGM may involve either two- or three-dimensional lattices. Here I shall initially apply the three-dimensional version to the entire material of a solid or liquid; except for situations with very high bulk concentration, finite size will only be of importance in an accumulation-type diffuse double layer, within two or three Debye lengths of the surface of an electrode, the interphase region. Even though a lattice model is somewhat of an artifice in the liquid case, employed to take finite charge carrier size into account, and more complicated approaches such as the use of the hypernetted chain approximation may be appropriate, the LGM reduces to the IGM in low concentration regions as it should; and, as concentration gets very high, an actual lattice structure should start to form even in a liquid. Thus the LGM is at least a reasonable second approximation for a liquid with free charge.

In high-concentration situations one must employ the following form of the Nernst-Planck flux equations [40]:

$$I_i = (-1)^{i+1} e [ (-1)^{i+1} \mu_i c_i \frac{d\psi}{dx} + D_i (c_i/a_i) \frac{da_i}{dx} ], \quad (6)$$

where the  $c_i$ 's are concentrations, the  $a_i$ 's are the corresponding activities, and  $\mu_i$  and  $D_i$  are mobilities and diffusion coefficients of the  $i$ th species, assumed concentration independent here. I have taken  $i=1$  for negative species (i.e.,  $c_1=n$ ) and  $i=2$  for positive ones. Let the common equilibrium bulk value of  $c_1$  and  $c_2$  be  $c_0$ . Here  $x$  is the distance in the material measured say from its beginning at the left end. The

quantity  $\psi$  is the inner potential (taken with reference to zero in the undisturbed bulk), and it is convenient to introduce the normalized potential  $\phi \equiv \psi/(kT/e)$ .

In a completely blocking situation ( $I_i = 0$ ), Eq. (6) yields quite generally  $a_i = a_{0i} \exp[(-1)^{i+1} \phi]$ . In the IGM,  $a_i = c_i$  and  $a_{0i} = c_0$ , giving the usual Boltzmann potential distribution for the concentrations. Free energy minimization in a completely blocking LGM equilibrium situation leads to [38,39] expressions for  $a_i$  in terms of  $c_i$  and  $c_i$  vs  $\phi$ . For the LGM,  $c_i$  is not Boltzmann distributed since its maximum cannot exceed  $N$ . Let us define  $\delta \equiv c_0/N$ , a fractional occupancy measure. Then for the solid LGM one finds  $a_i = c_i/[1 - (c_i/N)]$ ; thus  $a_{i0} = c_0/(1 - \delta)$ . Results of this kind are slightly more complicated for the liquid LGM.

Now for a partly blocking, direct-current-carrying situation one may invoke non-equilibrium thermodynamics to justify the use of the  $a_i$ 's found for thermal equilibrium in equations such as (6) with  $I_i = 0$ , provided the departures from equilibrium are not extreme. Thus, one can solve LGM equations for current-voltage, transient, and frequency-response results even under partially blocking nonlinear conditions, and, with the use of Butler-Volmer boundary conditions, obtain numerical results more realistic than those presented in Figs. 18-20. Such work remains to be done. Here it is worthwhile to contrast IGM and LGM predictions for completely blocking situations.

Consider the normalized charge density  $\rho^* = [\rho^* \{ \phi(x) \}]$  at some position  $x$ , taking  $\rho^* \equiv \rho/(eN)$ . The LGM leads to [39,41]

$$\rho^* = \frac{-2\delta(1-\chi\delta)\sinh(\phi)}{1 + 4\delta(1-\chi\delta)\sinh^2(\phi/2)} \quad (7)$$

where  $\chi \equiv 0$  for the liquid LGM and  $1$  for the Schottky-solid LGM. Here it is assumed that charges of both sign are mobile. There will be little difference between the two models unless  $\delta > 0.01$ . When  $\delta \rightarrow 0$ ,  $\rho^* \rightarrow -2\delta\sinh(\phi)$ , so that  $\rho = -(2ec_0)\sinh(\phi)$ , the usual IGM Gouy-Chapman result. But when  $|\phi| \rightarrow \infty$ , (7) leads to  $|\rho^*| = 1$ , a limited charge density. Some predictions of Eq. (7) are plotted in Fig. 21 for  $\chi = 0$  and several  $\delta$  values. The dashed lines are limiting IGM results. Clearly, the saturation region is reached for the LGM at larger  $\phi$  values the smaller  $\delta$ . To a good approximation the curve shapes are the same for  $\delta \gtrsim 0.1$ , and thus  $\rho^*(\phi_2) \approx \rho^*(\phi_1)$  if  $\phi_2 - \phi_1 = \ln(\delta_1/\delta_2)$ .

Now inclusion of nearest-neighbor electrostatic interactions in the free energy for the liquid LGM leads to the replacement of  $\phi$  in (7) by  $(\phi + \alpha\rho^*)$ , where  $\alpha$  is an interaction constant [41]. Of course, the modified Eq. (7) must then be solved self consistently for  $\rho^*$ , given  $\phi$ . This modification is more or less of the form Frumkin suggested heuristically long ago [42] for two-dimensional adsorption isotherms of the Langmuir form. It can arise from other sources as well as that mentioned above. When  $\alpha > 0$ , the approach of  $\rho^*$  to its saturated value as  $|\phi|$  increases is slower than that for  $\alpha = 0$ . But in both cases a finite and not very large  $\phi$  can lead to an extremely close approach to saturation, as shown

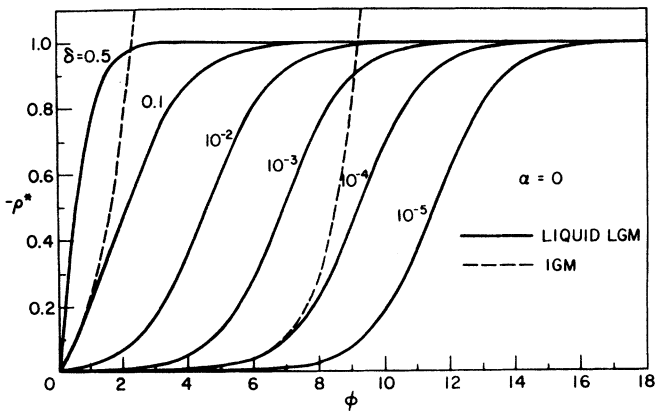


Fig. 21: The negative of the local normalized charge density  $\rho^*$  in the diffuse layer vs the normalized local average potential  $\phi$  showing the saturable character of the lattice gas model. Here  $\delta \equiv c_0/N$  is a fractional occupancy factor.

in Fig. 21 for  $\alpha = 0$ . If we write  $\rho^* \equiv \tanh(z)$ , indicating its saturable character, then the variable  $|z|$  will grow monotonically with  $|\phi|$ . But it is physically unrealistic to expect that at finite temperature a lattice could become essentially entirely filled with charges of a single sign either for solids or liquids. Therefore, it seems reasonable to consider a simple heuristic change in the feedback term  $\alpha\rho^* \equiv \alpha \tanh(z)$  to make the approach to saturation more drawn out. The one we shall use, one of the simplest possible, replaces the above with  $\alpha\rho^*/[1 - (\rho^*)^2]^{0.5} = \alpha \sinh(z)$ . Fig. 22 shows results for  $\delta = 10^{-3}$ , several values of  $\alpha$ , and both the  $\tanh(z)$  and  $\sinh(z)$  modifications. Indeed, the  $\sinh(z)$  term does not alter the  $\tanh(z)$  results much for small  $\delta$  but does lead to a more satisfactory asymptotic approach to saturation. The  $\sinh$  modification will probably be especially appropriate for solids, where the value of the normalized p.d. across the diffuse double layer  $\phi_d$  can be appreciable. In unadsorbed aqueous electrolytes, probably only rarely will  $\phi_d$  reach values where the distinction between the  $\tanh$  and  $\sinh$  modification terms will need to be made.

When  $\alpha = 0$ , it turns out that the Poisson equation incorporating the  $\rho^*$  of Eq. (7) can be integrated [39] for the situation of a completely blocking electrode at  $x = 0$ , normalized potential  $\phi_d$ , and an ohmic electrode at  $x = \infty$ , potential 0. One finds for the normalized field at  $x = 0$ ,

$$\epsilon_d = [\text{sgn}(\phi_d)] [\delta^{-1} \ln(1 + R_d)]^{0.5} \quad (8)$$

where

$$R_d \equiv 4\delta(1 - \chi\delta) \sinh^2(\phi_d/2), \quad (9)$$

and  $\epsilon_d \equiv E_d/(kT/eL_D)$ . Here  $L_D$  is the bulk Debye length and thus involves  $\epsilon_0$ . If  $\sigma_d$  is the total charge per unit area in the diffuse layer, then  $\epsilon \equiv \sigma/\sigma_n \equiv Q_d$ , where  $\sigma_n \equiv 2e\epsilon_0 L_D$ . Finally, the normalized differential capacitance of the diffuse layer is just  $C_{DON} \equiv C_{DO}/C_d \equiv -dQ_d/d\phi_d$ . Here  $C_d \equiv \epsilon_B/4\pi L_D$  is the IGM differential capacitance per unit area of the diffuse layer in the  $\phi_d \rightarrow 0$  limit. It involves  $\epsilon_B$ , the bulk dielectric permittivity. These relations lead, for  $\alpha = 0$ , to

$$C_{DON} = \frac{(1 - \chi\delta) \sinh|\phi_d|}{(1 + R_d) |\epsilon_d|}. \quad (10)$$

When  $\delta \rightarrow 0$ , Eq. (10) yields  $C_{DON} = \cosh(\phi_d/2)$ , the Gouy-Chapman result.

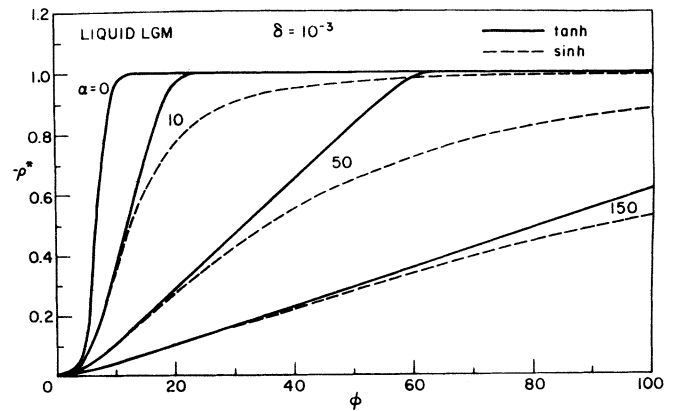


Fig. 22: The dependence of  $-\rho^*$  on  $\phi$  for three situations:  $\alpha = 0$ , no modification in the local charge-potential relationship;  $\alpha > 0$ ,  $\tanh$  and  $\sinh$  modifications--see text.

Fig. 23 shows how  $-Q_d$  varies with  $\phi_d$  for  $\delta = 10^{-3}$  and several  $\alpha$  values. As  $|\phi_d|$  becomes very large,  $Q_d$  becomes proportional to  $\sqrt{|\phi_d|}$ . The effect of increasing  $\alpha$  is to make a larger and larger portion of the response proportional to  $|\phi_d|^m$ , where  $m > 1$  and it approaches 1 for large  $\alpha$ . More details show up in the  $C_{DON}$  curves. Fig. 24 shows such results for various  $\delta$ 's and  $\alpha = 0$ . These curves were calculated for a Frenkel situation [39] and are thus asymmetric about  $\phi_d = 0$ . Results for the symmetric Schottky and liquid LGM situations are obtained, to very high accuracy, by reflecting the  $\phi_d \geq 0$  curves in the  $\phi_d = 0$  plane.

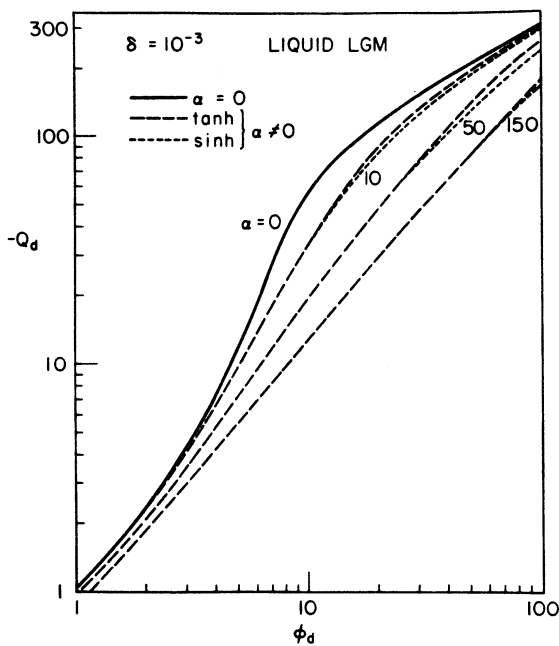


Fig. 23: The negative of the total normalized charge in the diffuse layer (charge per unit area),  $Q_d$ , vs  $\phi_d$  for  $\delta = 10^{-3}$  and various local charge-potential modifications.

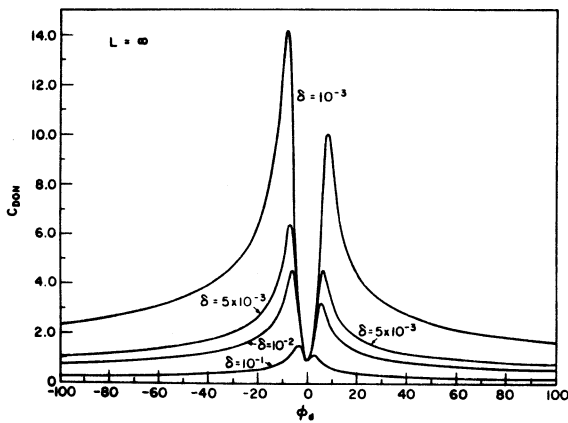


Fig. 24: The normalized differential capacitance of the diffuse layer,  $C_{DON}$ , vs the normalized p.d. across it,  $\phi_d$ , for various  $\delta$  values for a Frenkel-defect situation.

Most experiments will involve variation in  $\epsilon_0$  rather than  $N$ . Since  $C_d$ , used in normalizing  $C_{DON}$ , depends on  $\epsilon_0$ , it is of more interest to consider the variation of  $C_{DO}$ , the unnormalized diffuse layer differential capacitance, vs  $\delta$  and  $\phi_d$  (or  $\psi_d$ ) taking  $N$  as fixed. Such results for the liquid LGM are presented in Fig. 25 for parameter choices listed thereon. It is particularly interesting that the maximum values of  $C_{DO} \approx 150 \mu\text{F}/\text{cm}^2$ , are essentially independent of  $\delta$  for  $\delta \gtrsim 0.01$ . A IGM curve for  $\delta = 10^{-5}$  is also shown for comparison. Clearly, the peaks in  $C_{DO}$  are associated with the finite size of the charge carriers, directly related to the value of  $N$  chosen. Since  $C_d$  will vary as  $\sqrt{N}$  for fixed  $\delta$ , the larger  $N$ , the larger the maximum value of  $C_{DO}$ . Thus, if measurements of  $C_{DO}$  can be extended to sufficiently high  $\phi_d$  that the maximum of  $C_{DO}$  is defined, the experimental value of  $N$  may be readily determined. The same virtual  $\delta$  independence of the peak value of  $C_{DO}$  when  $\delta \gtrsim 0.01$  is found when  $\alpha \neq 0$  for either the tanh or sinh modifications.

Fig. 26 shows a few  $C_{DON}$  vs  $\phi_d$  results for fixed  $\delta$  and several  $\alpha$  values. Increasing  $\alpha$  decreases the peak  $C_{DON}$  and causes it to occur at higher  $\phi_d$ . The final decrease of  $C_{DON}$  is proportional to  $|\phi_d|^{-0.5}$ , as in Schottky junction depletion layers. The decrease arises from a quite different cause here; however, the near filling to saturation with charge of a single sign in a region of finite thickness next to the blocking electrode, a nearly saturated accumulation region.

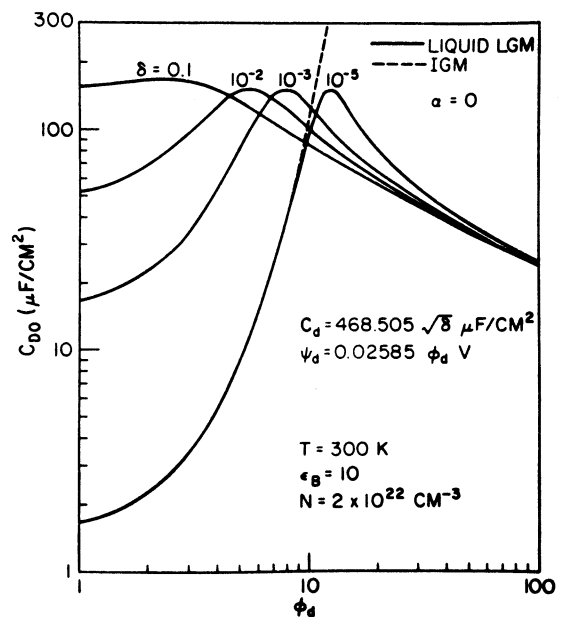


Fig. 25: The unnormalized differential capacitance per unit area of the diffuse layer,  $C_{DO}$ , vs  $\phi_d$  for various  $\delta$  values and  $\alpha = 0$ .

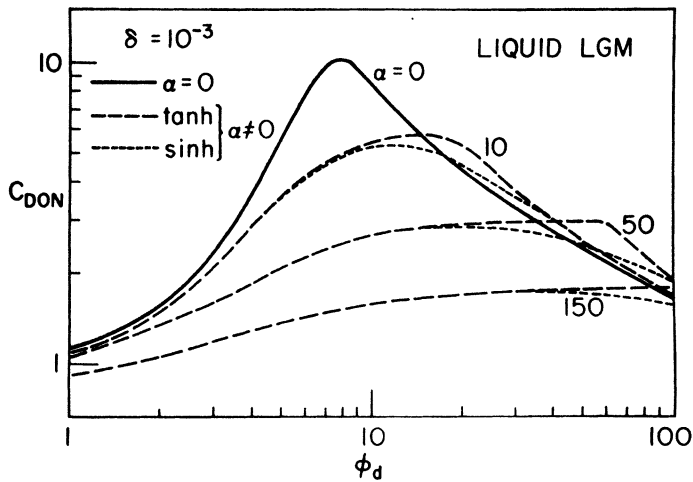


Fig. 26: The dependence of  $C_{DON}$  on  $\phi_d$  for  $\delta = 10^{-3}$  and various charge-potential modifications.

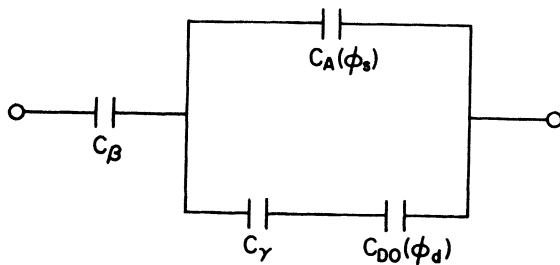


Fig. 27: Circuit showing the makeup of the total blocking-electrode differential capacitance,  $C_D$ , of a situation including surface adsorption at a finite number of surface sites, and with the finite size of ions taken into account in both the compact layer and the diffuse space charge region.

For charge carriers of finite size it is impossible to measure the diffuse layer capacitance,  $C_{DO}$ , directly because the charge centroids of the charged entities nearest the electrode will be separated from the mechanical surface of the electrode by about a radius of the charge carriers. Further, the effective electrical equipotential plane of the electrode will be of the order of 50 pm behind the mechanical surface because of field penetration effects. For an effective dielectric constant 3 of this inner compact layer, and a thickness of 15 pm, the capacitance which will therefore be in series with  $C_{DO}$  will be about 18  $\mu\text{F}/\text{cm}^2$ , limiting the overall measurable capacitance  $C_D$  to a maximum of this value, assuming complete blocking at the electrode.

When some of the charge carriers can take positions on specific sites on the electrode or at the surface of the material, they can be considered to be specifically adsorbed there. Then the diffuse layer begins to the right of these charges, and the inner layer, no longer charge-free, can be divided into two parts, leading to two essentially potential-independent capacitances which we shall designate as  $C_B$  and  $C_Y$ . When the adsorption isotherm for surface-adsorbed charges depends only on the local average potential at the centroids of these charges,  $\phi_s$ , it has been shown [39] that the overall capacitance of the system  $C_D$  is given by the circuit of Fig. 27, involving four separate capacitive elements. Two of these elements are potential-dependent. The resulting dependence of the overall capacitance on the applied potential difference,  $\psi_m$  at the electrode and zero at  $x = \infty$ , has been investigated [39] in some detail for a Frenkel case corresponding to single crystal AgCl. A final figure, Fig. 28, is presented here to show some of the complexity which can arise in such a situation. Here  $\delta$  is about  $10^{-5}$ ,  $\alpha = 0$ , and  $\Gamma_s$  is the number of kink sites on the surface of the crystal at which  $\text{Ag}^+$  ions may be "adsorbed." The structure of interest occurs in the region  $-1.5 < \psi_m < 1.5$  V, with 1.5 V equivalent here to a  $\phi_m$  of about 35. Note that the peak capacitance, arising primarily from adsorption, is displaced to the right from the  $\psi_m = 0$  point. Such displacement, associated with a constant term in the adsorption isotherm, arises because of the difference in free energies of formation of  $\text{Ag}^+$  interstitials and vacancies in AgCl.

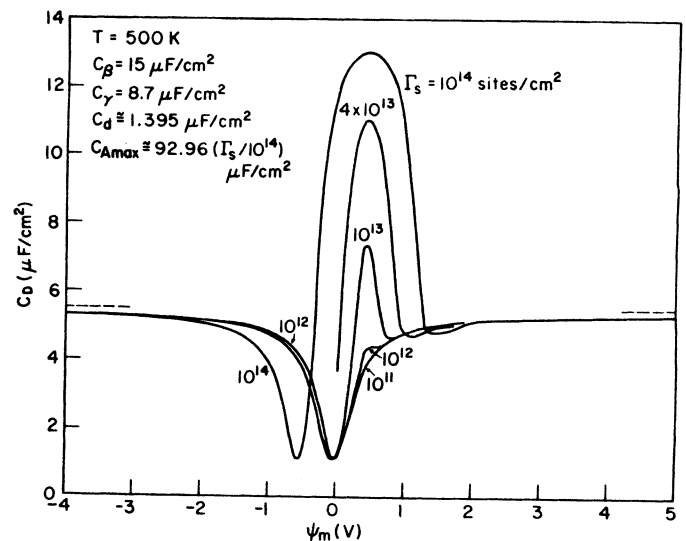


Fig. 28: The dependence of the total  $C_D$  of the specific adsorption situation of Fig. 26 on the p.d.,  $\psi_m$ , between the blocking electrode and an ohmic electrode at infinity. Here  $\Gamma_s$  is the surface density of available adsorption sites.

This review is not meant to give the impression that bulk and interphase charge motion effects are fully understood. Some understanding has indeed been gained, especially for the simplest cases, but much remains to be done. For example, a more detailed treatment of charge interactions, including neutral pair effects, is needed to provide an improvement over the Frumkin-like correction discussed above. Such micropotential calculations are needed both for charges in the diffuse layer and for specifically adsorbed charge. Much more work should be done on nonlinear response, with and without a static current present. Even the presence of built-in (Frenkel) diffuse space charge layers in interphase regions, a common occurrence, can lead to such nonlinearity. I hope, however, that this paper has provided the reader with a feeling for the scope and interest of the general area discussed.

#### ACKNOWLEDGMENTS

I wish to thank my three associates already mentioned for their crucial contributions to much of the work discussed. In addition, thanks are due to J. Schoonman for helpful comments and the use of his unpublished data. I also much appreciate the valuable work of John H. Dale in programming the 3-D plotting technique. Finally, I am grateful for N.S.F. support of much of this work under grants DMR75-10739, DMR76-84187, and DMR-8005236. Part of this work dealing with lattice gas models was presented at the San Jose, Calif. Workshop on Experimental and Theoretical Approaches to the Study of the Electrical Double Layer, 24 June 1980, and at the 158th meeting of the Electrochemical Society, Hollywood, Fla., 7 October 1980. Since presenting the present talk I have discovered that Gurevich and Kharkats have earlier considered lattice-gas space charge models with interactions between charges and found some results closely related to those herein (see *Sov. Phys. Chem. Dokl.* Vol. 229, 367 (1976) and *Solid State Comm.* Vol. 35, 1003 (1980)).

#### REFERENCES

- [1] W. B. Kowenhofen, "John Boswell Whitehead," *Biographical Memoirs*, Vol. 37, National Academy of Sciences, Columbia University Press, New York, 1964; pp. 343-361.
- [2] J. B. Whitehead, *Lectures on Dielectric Theory and Insulation*, McGraw Hill, New York, 1927.
- [3] J. B. Whitehead and W. Rueggeberg, *Trans. Am. Inst. Elect. Engrs.* Vol. 68, 520-524 (1949).
- [4] M. A. Lampert and P. Mark, *Current Injection in Solids*, Academic Press, New York, 1970.
- [5] B. Gross, 1978 Annual Report, 47th Conference on Electrical Insulation and Dielectric Phenomena, National Academy of Sciences, 1978; pp. 55-70.
- [6] B. Gross in *Topics in Applied Physics*, Vol. 33; Electrets, G. M. Sessler, Ed., Springer-Verlag, 1979; pp. 217-284.
- [7] A. K. Jonscher, *Nature* 267, 673-679 (1977). See also 1979 Annual Report, 48th Conference on Electrical Insulation and Dielectric Phenomena, National Academy of Sciences, 1979; pp. 393-413.
- [8] J. R. Macdonald and M. K. Brachman, *Rev. Mod. Phys.* Vol. 28, 393-422 (1956).
- [9] J. H. Calderwood and B. K. P. Scaife, 1977 Annual Report, 46th Conference on Electrical Insulation and Dielectric Phenomena, National Academy of Sciences, 1979; pp. 13-19.
- [10] G. M. Voglis, *Z. Phys.* Vol. 109, 52 (1938).
- [11] J. R. Macdonald, *J. Appl. Phys.* Vol. 32, 2385-2398 (1961).
- [12] K. L. Ngai, A. K. Jonscher, and C. T. White, *Nature*, Vol. 277, 185-189 (1979).
- [13] I. M. Hodge *et al.*, *J. Electroanal. Chem.* Vol. 58, 429 (1975).
- [14] J. R. Macdonald, *J. Chem. Phys.* Vol. 54, 2026-2050 (1971).
- [15] J. R. Macdonald in *Electrode Processes in Solid State Ionics*, edited by M. Kleitz and J. Dupuy, Reidel Publishing Company, Dordrecht-Holland, 1976; pp. 149-183.
- [16] K. S. Cole and R. H. Cole, *J. Chem. Phys.* Vol. 9, 341 (1941).
- [17] J. R. Macdonald and D. R. Franceschetti, *J. Chem. Phys.* Vol. 68, 1614-1637 (1978).
- [18] D. R. Franceschetti and J. R. Macdonald, *J. Electroanal. Chem.* Vol. 82, 271-301 (1977).
- [19] J. R. Macdonald and D. R. Franceschetti, *J. Electroanal. Chem.* Vol. 99, 283-298 (1979).
- [20] J. R. Macdonald and J. A. Garber, *J. Electrochem. Soc.* Vol. 124, 1022-1030 (1977).
- [21] D. R. Franceschetti and J. R. Macdonald, *J. Electroanal. Chem.* Vol. 101, 307-316 (1979).
- [22] J. R. Macdonald, *J. Electroanal. Chem.* Vol. 32, 317-328 (1971) and references therein.
- [23] E. Warburg, *Ann. Phys. Chem.* Vol. 67, 493 (1899).
- [24] S. H. Glarum and J. H. Marshall, *J. Electrochem. Soc.* Vol. 127, 1467-1474 (1980).
- [25] J. R. Macdonald, *J. Chem. Phys.* Vol. 58, 4982-5001 (1973).
- [26] D. R. Franceschetti and J. R. Macdonald in *Proceedings of the Third Symposium on Electrode Processes*, Vol. 80-3, edited by S. Bruckenstein *et al.*, The Electrochemical Society, Princeton, N. J. 1980; pp. 94-114.
- [27] J. R. Macdonald, *J. Electroanal. Chem.* Vol. 53, 1-55 (1974).

- [28] J. R. Macdonald in *Superionic Conductors*, edited by G. D. Mahan and W. L. Roth, Plenum Publishing Co., New York, 1976; pp. 81-87.
- [29] R. D. Armstrong, M. F. Bell, and A. A. Metcalfe, in *Specialist periodical Reports - Electrochemistry*, Vol. 6, The Chemical Society, London, 1978; pp. 98-127.
- [30] W. I. Archer and R. D. Armstrong in *Specialist Periodical Reports - Electrochemistry*, Vol. 7, The Chemical Society, London, 1979; pp. 157-202.
- [31] J. R. Macdonald, *J. Electroanal. Chem.* Vol. 70, 17-26 (1976).
- [32] C. Gabrielli, Thesis, University of Paris, No. C.N.R.S. A.O. 8060: *Metaux, Corrosion, Industrie*, No. 573, 574, 577, 578 (1973). See p. 82 in thesis.
- [33] J. R. Macdonald, D. R. Franceschetti, and R. Meaudre, *J. Phys. C: Solid State Phys.* Vol. 10, 1459-1471 (1977).
- [34] D. R. Franceschetti and J. R. Macdonald *J. Appl. Phys.* Vol. 50, 291-302 (1979).
- [35] D. R. Franceschetti and J. R. Macdonald, *J. Electroanal. Chem.* Vol. 100, 583-605 (1979).  
*[The  $X/2$  terms in Eqs. 21 and 22 should be replaced by  $X$  and the  $\coth(M)$  term in Eq. 26 replaced by  $\coth(2M)$ .]*
- [36] G. Gouy, *J. Phys.* Vol. 9, 457 (1913).
- [37] D. L. Chapman, *Phil. Mag.* Vol. 25, 475 (1913).
- [38] T. B. Grimley, *Proc. Roy. Soc. (London)* Vol. 201A, 40-61, (1950).
- [39] J. R. Macdonald, D. R. Franceschetti, and A. P. Lehnen, *J. Chem. Phys.* Vol. 73, 5272-5293, (1980).
- [40] W. Weppner and R. A. Huggins, *Ann. Rev. Mat. Sci.* Vol. 8, 269-311 (1978).
- [41] J. R. Macdonald, D. R. Franceschetti, and A. P. Lehnen, submitted to *J. Phys. Chem. Solids*.
- [42] A. N. Frumkin, *Z. Physik* Vol. 35, 792-802 (1926).

*This paper was presented on 27 October 1980 as the J. B. Whitehead Memorial Lecture of the 1980 Conference on Electrical Insulation and Dielectric Phenomena, Parker House, Boston, Massachusetts.*

*Manuscript was received 12 December 1980.*